



Cite this: *Nanoscale*, 2024, **16**, 4787

## Unexpectedly high thermal stability of Au nanotriangle@mSiO<sub>2</sub> yolk–shell nanoparticles†

Xiaobin Xie, \*‡, Wiebke Albrecht, §, Marijn A. van Huis \* and Alfons van Blaaderen\*

The shape of Au nanoparticles (NPs) plays a crucial role for applications in, amongst others, catalysis, electronic devices, biomedicine, and sensing. Typically, the deformation of the morphology of Au NPs is the most significant cause of loss of functionality. Here, we systematically investigate the thermal stability of Au nanotriangles (NTs) coated with (mesoporous) silica shells with different morphologies (core–shell (CS): Au NT@mSiO<sub>2</sub>/yolk–shell (YS): Au NT@mSiO<sub>2</sub>) and compare these to ‘bare’ nanoparticles (Au NTs), by a combination of *in situ* and/or *ex situ* TEM techniques and spectroscopy methods. Au NTs with a mesoporous silica (mSiO<sub>2</sub>) coating were found to show much higher thermal stability than those without a mSiO<sub>2</sub> coating, as the mSiO<sub>2</sub> shell restricts the (self-)diffusion of surface atoms. For the Au NT@mSiO<sub>2</sub> CS and YS NPs, a thicker mSiO<sub>2</sub> shell provides better protection than uncoated Au NTs. Surprisingly, the Au NT@mSiO<sub>2</sub> YS NPs were found to be as stable as Au NT@mSiO<sub>2</sub> CS NPs with a core–shell morphology. We hypothesize that the only explanation for this unexpected finding was the thicker and higher density SiO<sub>2</sub> shell of YS NPs that prevents diffusion of Au surface atoms to more thermodynamically favorable positions.

Received 21st November 2023,  
Accepted 17th January 2024

DOI: 10.1039/d3nr05916b

rsc.li/nanoscale

## Introduction

Au nanoplatelets (Au NPLs) have increasingly attracted interest because of their promising application in various fields, such as sensing,<sup>1,2</sup> biology,<sup>3,4</sup> and catalysis.<sup>5–7</sup> The shape stability of Au NPLs plays a significant role in their functionality,<sup>8</sup> in particular for those applications based on their plasmonic properties, for example, for optothermal effects, plasmonic enhanced photocatalysis and sensing which rely on the strong electromagnetic field enhancements that result specifically at the sharp tips of these particles. Being one of the non-equilibrium morphologies, plate-like nanoparticles with pointed tips like triangles easily lose their shape which subsequently leads to a significant loss of functionality. Therefore, understanding the deformation mechanism and developing a solution providing enhanced shape stability are of major importance for the use of these systems in many fields.

Recent developments associated with the *in situ* heating TEM technique in which thin electron transparent windows are used and heating cells can be combined with microfluidic techniques enable real time observations of various dynamic processes of materials under different atmospheric conditions.<sup>9–13</sup> By using *in situ* heating TEM, van der Hoeven *et al.*<sup>14</sup> investigated alloying and atomic diffusion in bimetallic Au@M (Ag, Pd, Pt) nanorods in a vacuum and obtained fully alloyed bimetallic nanorods. Also, Prof. Bals’ group demonstrated several cases of shape evolution and atom diffusion in Au-based (bi)metallic nanoparticles by combining tomography and *in situ* heating TEM.<sup>15–17</sup> X. Pan *et al.*<sup>18</sup> studied the dynamics and surface composition of face-dependent oxidation of Pt<sub>3</sub>Co nanoparticles *via* the *in situ* gas cell TEM technique and revealed that Co segregation and oxidation occur on {111} surfaces other than {100} surfaces.

To date, most of the reports on the thermal stability and/or reshaping of Au nanoparticles (NPs) have focused on spherical,<sup>19</sup> cubic,<sup>20</sup> rod-like shapes,<sup>21–24</sup> and their core–shell coating structures.<sup>17,25</sup> Among the previous works, the size-dependent melting points of Au nanospheres (NSs) and Au NS@mSiO<sub>2</sub> were revealed by P. Buffat *et al.*<sup>26</sup> and D. Meisel and co-workers,<sup>27</sup> respectively. Furthermore, the thermal stability of nanoplates with large sizes, up to 50 μm, was studied by Kan *et al.*<sup>8</sup> and they found that heating to 600 °C induces the fragmentation of Au NPLs into small pieces. Recently, R. Wang and D. Kurouski reported three possible routes for the thermal

*Soft Condensed Matter, Debye Institute for Nanomaterials Science, Utrecht University, Princetonplein 5, 3584 CC Utrecht, The Netherlands.*

*E-mail: x.xie@hotmail.com, m.a.vanhuis@uu.nl, a.vanblaaderen@uu.nl*

† Electronic supplementary information (ESI) available. See DOI: <https://doi.org/10.1039/d3nr05916b>

‡ Present Address: Analytical & Testing Center, Sichuan University, Chengdu 610064, China.

§ Present Address: Department of Sustainable Energy Materials, AMOLF, Science Park 104, 1098 XG Amsterdam, The Netherlands.

reshaping of Au microplates 15–20  $\mu\text{m}$  long and 30 nm or 60 nm thick, wherein they found that walled Au NPLs, concave Au NPLs, and invariable Au NPLs could be obtained at 300  $^{\circ}\text{C}$  and almost all of the particles transformed into walled Au NPLs at 500  $^{\circ}\text{C}$ .<sup>28</sup> Additionally, H. Cho *et al.* revealed the atomic dynamics of Au NRs and Au NPLs under a 1 mbar oxygen atmosphere *via* environmental TEM, which showed that Au NRs tended to become ellipsoids while triangular Au NPLs transformed into a  $\{111\}$  facet-enclosed hexagonal shape.<sup>29</sup> Moreover, a recent paper indicates that with a rigid surface coating of silica, Au@Ag NRs and Au@Ag NTs showed enhanced thermal stability, which even enabled the determination of the diffusion constants in single bimetallic nanoparticles as a function of shape.<sup>17</sup> The mentioned thermal stability studies on surface-coated Au NPs mainly focused on core-shell geometries. Recent investigations on hetero-catalytic reactions indicated that the presence of metal catalysts in a yolk-shell coating structure could significantly enhance their catalytic performance.<sup>30–36</sup> However, not much is known about the thermal stability of yolk-shell structures although the different geometry likely alters the thermal stability and reshaping mechanism.

In this work, we systematically investigated the thermal stability of Au NTs with different forms of coatings and coating-geometries, namely Au NT-CTAC, Au NT@mSiO<sub>2</sub> core-

shell (CS) NPs and Au NT@mSiO<sub>2</sub> yolk-shell (YS) NPs. *In situ* transmission electron microscopy (TEM) heating techniques were used for monitoring the deformation process within a temperature range of 20  $^{\circ}\text{C}$ –1100  $^{\circ}\text{C}$ , while *ex situ* oven heating combined with scanning transmission electron microscopy (STEM) and ultraviolet-visible (UV-VIS) spectroscopy was also used for the analysis of the thermal stability from 20  $^{\circ}\text{C}$  to 600  $^{\circ}\text{C}$ . We found that the Au NTs started to deform at around 200  $^{\circ}\text{C}$  and the deformation occurred at the corners and edges where the atoms' coordination number is lower than at other positions in the particles. The Au NT shape stability was found to be significantly enhanced by a mesoporous silica (mSiO<sub>2</sub>) shell coating, and a thicker shell provided better stability, as was already observed before for rod-shaped Au nanoparticles as well.<sup>23</sup> Interestingly, both the Au NT@mSiO<sub>2</sub> YS NPs and the Au NT@mSiO<sub>2</sub> CS NPs displayed a similarly high thermal stability despite the fact that in the case of the YS morphology the Au NTs were only partially covered by a thicker silica shell. We speculate how this counterintuitive finding can be explained.

## Results and discussion

The Au NTs were synthesized by modification of a previously reported protocol.<sup>1</sup> The as-prepared single crystalline Au NTs

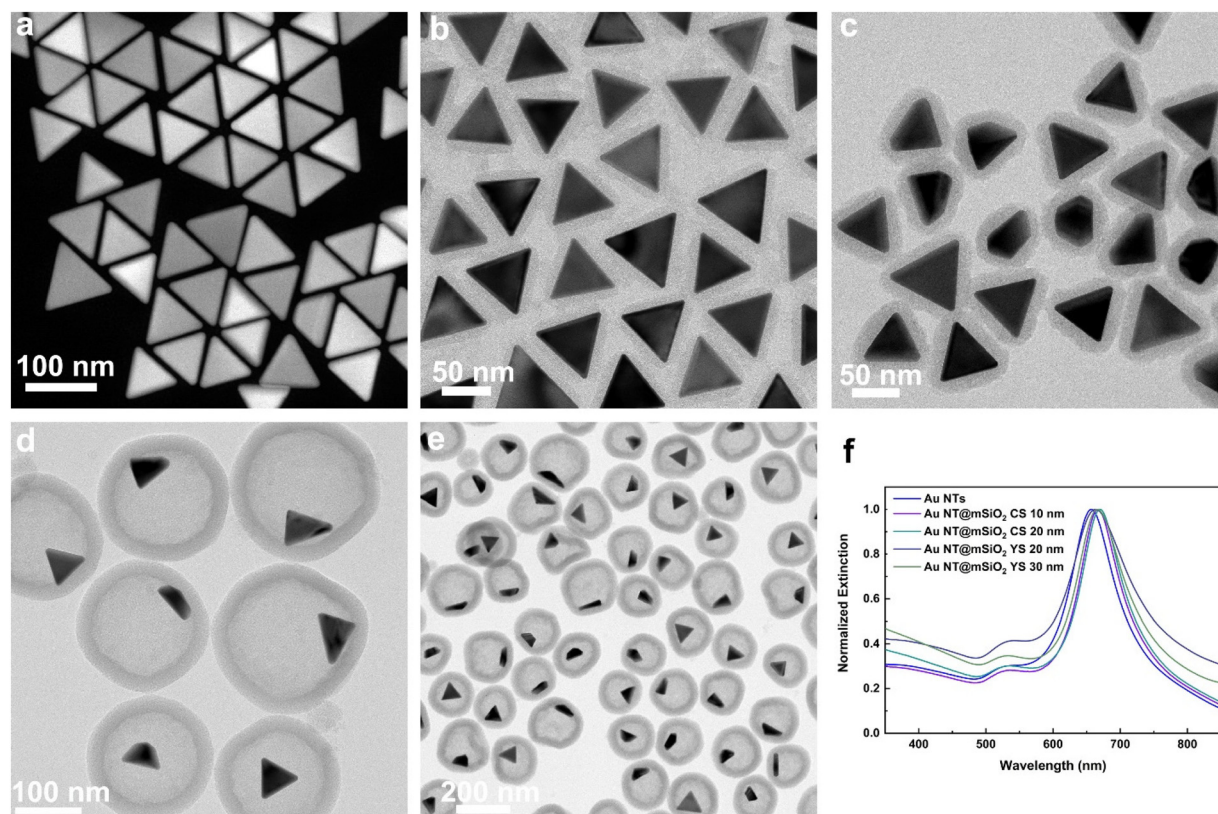


**Fig. 1** Characterization of Au NTs, Au NT@mSiO<sub>2</sub> core shell and yolk shell NPs. (a) STEM image of Au NT, (b) TEM image of Au NT@mSiO<sub>2</sub> CS NPs with 10 nm SiO<sub>2</sub> shell, (c) TEM image of Au NT@mSiO<sub>2</sub> CS NPs with 20 nm SiO<sub>2</sub> shell, (d) TEM image of Au NT@mSiO<sub>2</sub> yolk-shell (YS) NPs with 20 nm SiO<sub>2</sub> shell, (e) TEM image of Au NT@mSiO<sub>2</sub> yolk-shell (YS) NPs with 30 nm SiO<sub>2</sub> shell and (f) UV-VIS spectra of the NPs presented above.

had a well-defined triangular shape, with an average edge-length of 66 nm and a thickness of 22 nm (Fig. 1a). Fig. S1† shows views at different angles and high-resolution TEM (HRTEM) images of Au NTs, revealing that the face centered cubic (FCC) Au NTs are lamellar twinned particles, and each Au NT is enclosed by six  $\{100\}$  facets at their sides and two  $\{111\}$  facets on the top and bottom. The Au NT@mSiO<sub>2</sub> CS and YS NPs were prepared according to the methods presented in a recent report by us.<sup>37</sup> As shown in Fig. 1b and c, the coating of the Au NTs with a mSiO<sub>2</sub> shell of thicknesses of 10 nm and 20 nm was successful. Fig. 1d and e show the clear yolk-shell structure of Au NT@mSiO<sub>2</sub> YS NPs, where the shell thickness was about 20 nm and 30 nm in panel d and e, respectively. The average pore size of these mSiO<sub>2</sub> shells was found to be about 0.7 nm and 0.6 nm for core-shell and yolk-shell particles, respectively (Fig. S2†). Moreover, there is no evidence of mSiO<sub>2</sub> covering the free surfaces of the Au NTs in the yolk-shell particles, from HRTEM images of Au NT@mSiO<sub>2</sub> YS NPs displayed in Fig. S3.† Our liquid-cell TEM experiments indicated that the Au NT cores were stuck after synthesis with one of their sides onto the porous outer shell mSiO<sub>2</sub> shells (Movie S1, ESI†). The localized surface plasmon resonance (LSPR) bands of the Au NT@mSiO<sub>2</sub> CS and YS NPs showed a slight red shift compared to the Au NTs (Fig. 1f) because the refractive index of the mSiO<sub>2</sub> shell is higher than that of H<sub>2</sub>O slightly shifting the plasmon resonance frequency.<sup>38</sup>

First, we investigated the thermal stability of the Au NTs without a silica coating using *in situ* heating STEM. The experimental details can be found in the Experimental section. One point should be noted that we used a camera length of 98 mm for all STEM imaging to reduce diffraction contrast and mSiO<sub>2</sub> shells of Au NT@mSiO<sub>2</sub> particles were invisible under this condition (Fig. S4†). Fig. S5† shows the heating procedure corre-

sponding to the images presented in Fig. 2 and Fig. S6,† which allows us to trace the heating process of the *in situ* heating TEM experiments, since the switching to different windows, adjusting imaging focus, recording movies and sometimes the vibrations during the experiments are all taken times. Fig. 2 shows the high angle annular dark field – scanning transmission electron microscopy (HAADF-STEM) images of different Au NTs on different SiN<sub>x</sub> windows acquired at each set temperature. It is important to mention that we are aware of the effects that can influence the thermal stability of nanoparticles when they are investigated by electron microscopy that are easily missed. For instance, it was recently investigated and shown by some of us how organic molecules like ligands can be transformed by an electron beam into a thin, hard-to-observe carbon layer with a thickness around ~1 nm that strongly enhances the thermal stability, easily for several hundreds of degrees, of Au nanoparticles.<sup>39</sup> Thus our measurements in the present paper were always compared with *ex situ* measurements and under conditions under which such effects were minimized. The corners and edges of the Au NTs became rounded at around 200 °C, and the top and bottom crystal planes, consisting of  $\{111\}$  facets, became uneven upon increasing the temperature (which became apparent from the changing contrast of the STEM images), and the particles finally transformed into more spherical shapes. For the images discussed, all the Au NTs were not exposed to the electron beam during the heating before imaging, which minimizes the influence of the electron beam.<sup>39</sup> In contrast, those particles that had been exposed to the electron beam before heating became stable to changes in shape for 800 degrees, and the way of deformation was altered (Fig. S6†). The reason for this is that the CTAC surfactant molecules, covering the Au NT surfaces, turned into a thin carbon layer once exposed to the electron beam. These carbon layers can dramatically enhance the thermal stability of Au NPs during *in situ* heating TEM experiments, which was recently investigated in detail.<sup>39</sup>

To further reveal the factors affecting the deformation of the Au NTs and to check for artefacts caused by the imaging and/or the atmospheric and substrate conditions, the particles were heated in thermal tests with *ex situ* heating of the same batch of Au NTs at different temperatures of 200 °C, 300 °C, and 400 °C, under both air and N<sub>2</sub> atmospheres, for one hour. The Au NTs were dropcast onto TEM grids that were covered by a SiO<sub>x</sub>-film and then heated in an oven (more details of the experiments are provided in the ESI†). The results were similar to the results of the *in situ* TEM heating, and the deformation occurred from the corners and edges of the Au NTs (Fig. 2) at similar temperatures. Nearly all the Au NTs turned into sphere-like NPs after heating at 400 °C for one hour in air, and when heating following a similar temperature-increase program to 400 °C under N<sub>2</sub> (Fig. S7†), which also means that differences caused by the air and N<sub>2</sub> environments were negligible in this case. The shape of Au NTs after cooling in the oven heating experiments might be different from their shape at the heating temperature. The exact shape transformations during cooling remain unknown in these experiments.

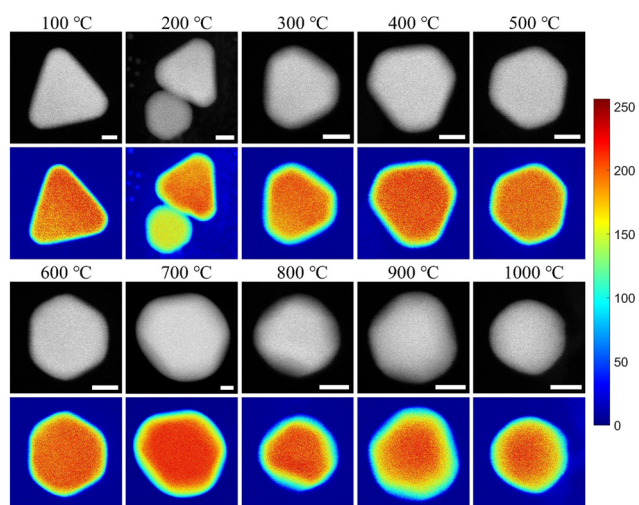


**Fig. 2** *In situ* heating study of Au NTs. STEM images acquired at different temperatures and their corresponding color maps indicate the shape evolution of Au NT with increasing the heating temperature. The scale bar present 50 nm, and the color bar shows the brightness contrast.

Nevertheless, we expect them to be small due to the short cooling time compared to the 1 h heating time. The important point is that the whole process leads to a more thermodynamically stable shape which was similar in all cases based on observations from the *in situ* and *ex situ* heating experiments. To exclude effects of the substrate, Au NTs on *in situ* heating chips ( $\text{SiN}_x$  substrate) and TEM grids ( $\text{SiO}_x$  substrate) were heated in an oven at 400 °C for one hour in air as well. As shown in Fig. S8,<sup>†</sup> all Au NTs became more sphere-like particles on both substrates, which means the substrates did not influence the experiments in this work either.

To further gain insights into how incomplete surface coatings influence the thermally induced deformation of the Au NTs, we performed an *in situ* heating TEM experiment on Au NT@mSiO<sub>2</sub> CS NPs coated with an ~10 nm mesoporous mSiO<sub>2</sub> shell. Such mesoporous shells can stabilize Au nanoparticles, while still providing access to the Au surface which can be important for applications like sensing and catalysis. The temperature–time function of the heating process is shown in Fig. S9.<sup>†</sup> The temperature was increased to 1100 °C in 120 min, and a typical morphology evolution process of Au NT@mSiO<sub>2</sub> CS NPs is shown in Fig. S10 and S11.<sup>†</sup> The edges and corners of the Au NTs became rounded as the temperature increased; however, for those without exposure to an electron beam before, the triangular shape remained until 650 °C and for those exposed to an electron beam from the beginning of the experiment, the triangular shape remained until 1000 °C. This is slightly higher than was observed for mesoporous silica-coated rod-shaped Au NPs.<sup>24,39</sup> At 1050 °C, the STEM image and its intensity profiles across the particle indicate that the center of the Au NT had become thicker than the edge and no longer retained its plate-like shape (Fig. S12<sup>†</sup>). As the temperature was increased to 1100 °C, which is higher than the melting point of bulk gold (1064 °C),<sup>27</sup> the mSiO<sub>2</sub> shell

was broken and the Au NTs vaporized (ESI Movie S2<sup>†</sup>). Based on the above findings, the mSiO<sub>2</sub> shell significantly enhanced the shape stability of Au NTs, which is in agreement with previous reports on other mSiO<sub>2</sub> coated nanoparticles, however, even to temperatures higher than of several other anisotropic shapes.<sup>25,40</sup> We speculate that the stronger effectiveness of the mesoporous silica layer to prevent shape changes to the NTs in this study is due to both the fact that at some elevated temperature ~750 °C<sup>25</sup> (the exact temperature depends on many details such as the thickness of the silica layer and synthesis conditions) the pores inside the silica will be closed and the Au NP becomes covered by a closed silica layer. That such a complete silica layer is more effective in hindering the diffusion of Au atoms over the surfaces of the particles is not surprising also given our earlier findings on the role of thin carbon layers that also can prevent shape changes up to very high temperatures close to the melting point of bulk Au.<sup>39</sup> Apparently, the morphology of the Au NTs with their flat faces hinders Au diffusion by a complete silica coating that is necessary to change the NP shape more effectively than for example that of Au NRs.<sup>29</sup>

In order to investigate the effects of the thickness and structure of the mSiO<sub>2</sub> shell, more *ex situ* heating experiments were carried out on Au NT@mSiO<sub>2</sub> CS NPs with a shell thickness of ~10 nm (marked as Au NT@mSiO<sub>2</sub> CS-10) and ~20 nm (marked as Au NT@mSiO<sub>2</sub> CS-20). First, we heated the Au NT@mSiO<sub>2</sub>-10 and Au NT@mSiO<sub>2</sub>-20 samples in the oven in air at 400 °C for one hour and for three hours. It is well known that the localized surface plasmon resonance (LSPR) of Au NPLs is a strong function of the particle shape.<sup>41</sup> Blue-shifts happen to their LSPR bands as their sharp tips become rounded. Thus, the LSPR bands of these samples were measured before and after heating. As shown in Fig. S13,<sup>†</sup> the LSPR bands of Au NT@mSiO<sub>2</sub>-10 shifted more strongly than

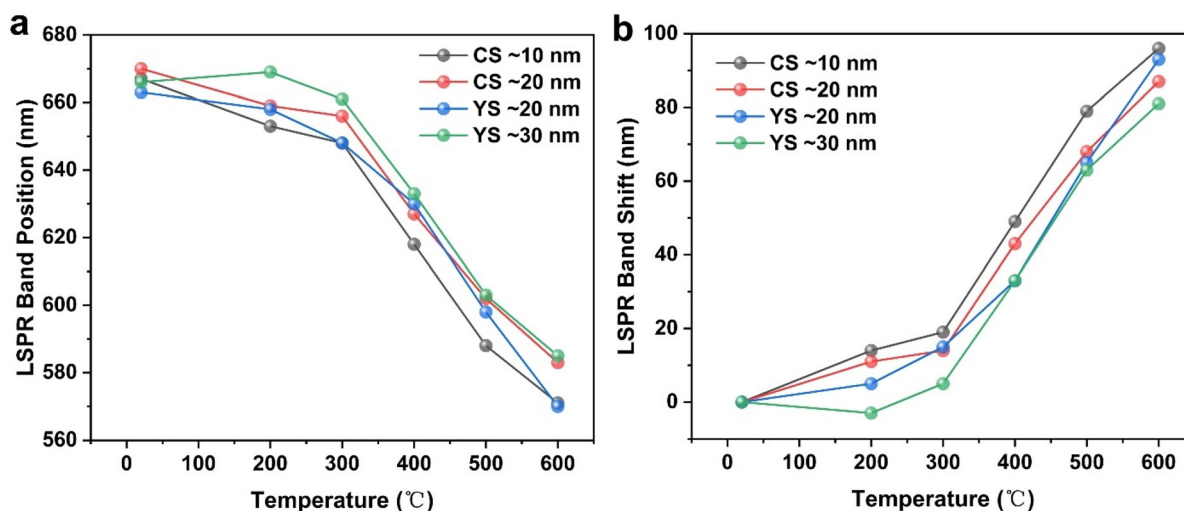
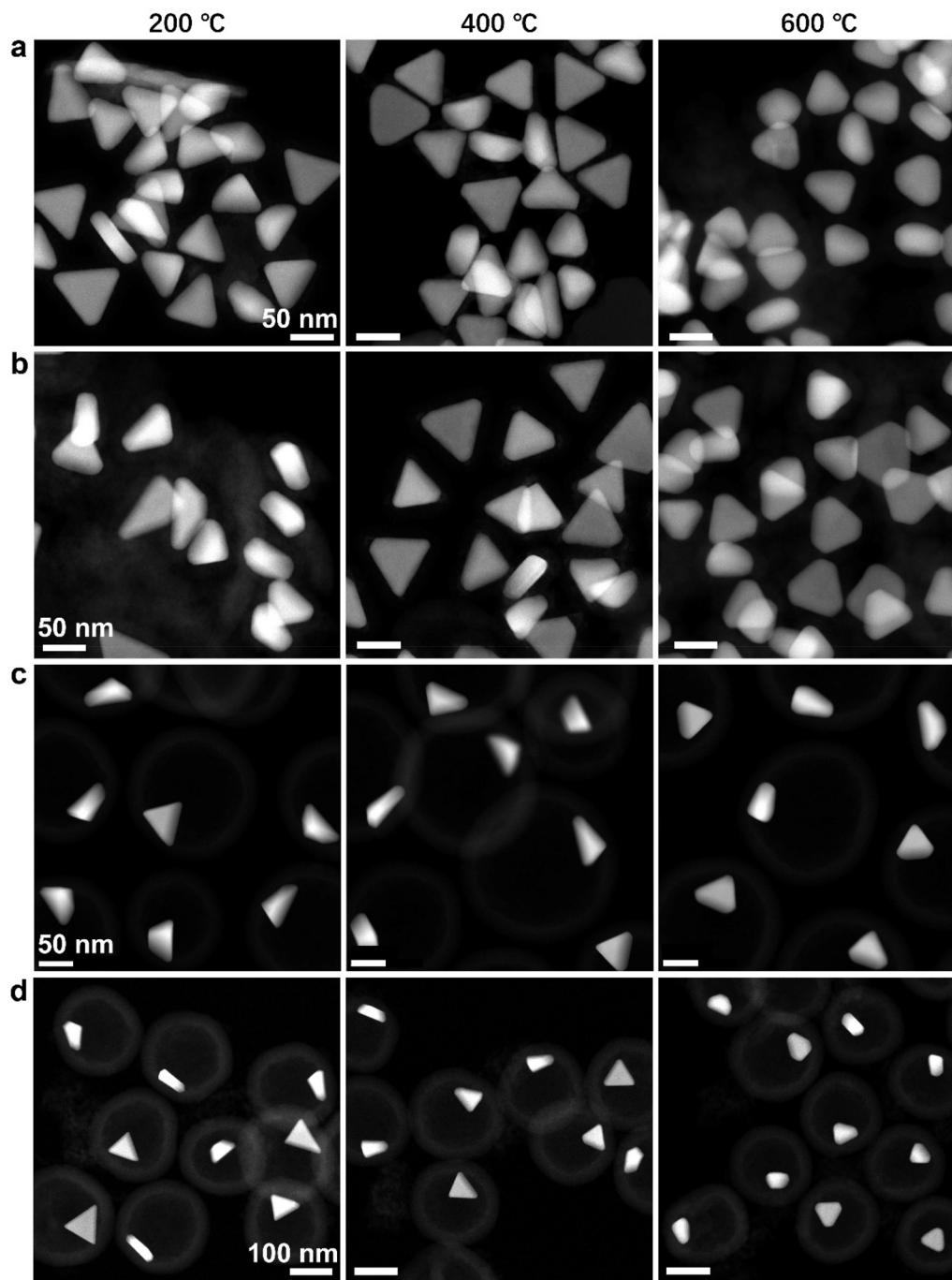


Fig. 3 The changes of localized surface plasmon resonance (LSPR) of Au NT@mSiO<sub>2</sub> CS and YS NPs before and after heating at different temperatures in an oven in air. (a) LSPR band positions and (b) LSPR band shifts of the heated Au NT@mSiO<sub>2</sub> CS and YS NPs.

those of Au NT@mSiO<sub>2</sub>-20. As the heating time increased, the LSPR bands shifted more. The corresponding STEM image of each heating point is shown in Fig. S14,<sup>†</sup> which together with the LSPR band shifts clearly indicates that the Au NT@mSiO<sub>2</sub>-20 system was more stable than the Au NT@mSiO<sub>2</sub>-10 system.

To further reveal the effects caused by differences in the mSiO<sub>2</sub> coatings and effects of the shell morphology, Au

NT@mSiO<sub>2</sub> CS-10, Au NT@mSiO<sub>2</sub> CS-20, and Au NT@mSiO<sub>2</sub> YS NPs with a shell thickness of ~20 nm (marked as Au NT@mSiO<sub>2</sub> YS-20) and ~30 nm (marked as Au NT@mSiO<sub>2</sub> YS-30) were heated at different temperatures for one hour in an oven in air. The LSPR bands are shown in Fig. S15<sup>†</sup> and the positions and shifts of the bands are summarized in Fig. 3. In comparison with their original LSPR band, slight blue shifts of



**Fig. 4** Shape evolution of Au NT@mSiO<sub>2</sub> CS and YS NPs before and after heating at different temperatures in an oven in air. (a) STEM images of Au NT@mSiO<sub>2</sub> CS-10 nm; (b) STEM images of Au NT@mSiO<sub>2</sub> CS-20 nm; (c) STEM images of Au NT@mSiO<sub>2</sub> YS-20 nm; (d) STEM images of Au NT@mSiO<sub>2</sub> YS-30 nm. The scale bar indicates 50 nm in a, b and c, 100 nm in d.

the plasmon peak of all three types of mSiO<sub>2</sub> coated Au NTs were found after heating at 200 °C and 300 °C, while a dramatic blue shift of the LSPR bands occurred when the experimental temperatures were increased to 400 °C and higher, which clearly indicates deformation of the Au NTs. Our FDTD simulations of the LSPR bands of Au NTs and deformed Au NTs confirm that the deformation of the Au NTs leads to similar blue shifts of LSPR bands (Fig. S16†). Moreover, the STEM images of all four types of NPs after heating at 200 °C, 400 °C, and 600 °C provided direct evidence of the deformation of the Au NTs (Fig. 4). The TEM images of the NPs after heating at 600 °C indicate that the structural stability of the mSiO<sub>2</sub> shells is still well retained after heating (Fig. S17†). For the YS as well as the CS shells, it appears that the porosity of the SiO<sub>2</sub> decreased (Fig. S17†), which likely enhances the thermal stability. From the edge length distributions of heated Au NTs in Fig. 5, the order of average edge length of Au cores of these four types of coating is Au NT@mSiO<sub>2</sub> YS-30 (~46.4 nm) > Au NT@mSiO<sub>2</sub> CS-20 (~45.0 nm) > Au NT@mSiO<sub>2</sub> YS-20 (~44.5 nm) > Au NT@mSiO<sub>2</sub> CS-10 (~43.5 nm). There is no doubt that a thicker mSiO<sub>2</sub> shell provided better protection for the Au NT cores because of the stronger mechanical properties of thicker shells. But, surprisingly, the Au NT@mSiO<sub>2</sub> YS NPs were somehow as stable as the core-shell NPs.

To understand the unexpected results on the high shape stability of the YS Au NT@mSiO<sub>2</sub> in comparison with the other Au NTs systems, we will briefly go over both the role of the

thermodynamic driving forces driving the out-of-equilibrium shapes of the NPs back to a more spherical shape and the kinetic factors influencing the speed of this process in the following: first, the volume and surface area of a triangular *versus* spherical shape can be calculated *via* simply considering their geometrical shape as the particles' size here is large enough to ignore the real atomic structure on the physical surface areas.<sup>42</sup> As shown in Table S2,† the surface area to volume ratio reduces from 0.18 nm<sup>2</sup> nm<sup>-3</sup> for the Au NTs given the average experimental values to 0.15 nm<sup>2</sup> nm<sup>-3</sup> for a spherical shape of the same volume, and the specific surface area of the particle decreases from 9.3 m<sup>2</sup> g<sup>-1</sup> to 7.8 m<sup>2</sup> g<sup>-1</sup> when the shape changes from a triangle to a sphere. Furthermore, the total Gibbs free energy of the Au NPs can be approximated using the following expression:<sup>20</sup>

$$G^{\text{total}} = \Delta_f G^0 + \frac{M}{\rho} (1 - e) \left[ q \sum_i f_i \gamma_i \right] \quad (1)$$

where  $\Delta_f G^0$  is the standard formation free energy of bulk Au which is indicated by the 0 superscript here,  $\rho$  is the density of Au,  $M$  is the molar mass,  $e$  denotes a volume dilation caused by surface stress and assumed it is the same for both Au particles here, and  $q$  is the surface-to-volume ratio. The surface free energy of each crystal surface  $i$  is expressed as  $\gamma_i$  and assigned weight with a corresponding factor  $f_i$ . It should be pointed out that the energetic contributions from the edges and corners have been ignored here as the size of the Au NPs is much larger than 3 nm.<sup>20</sup> A comparison of the total Gibbs free energy of the Au NTs and Au NSs was made by using the surface energies shown in Table S1† and the surface to volume ratio we calculated above, and it follows that  $G^{\text{total}}(\text{Au NT})/G^{\text{total}}(\text{Au NS}) = 1.28$ . This calculation provides the driving force for the deformed Au NTs transforming into a more sphere-like shape and how much free energy is gained by this transformation.

In accordance with the above theoretical considerations, the deformation of Au NTs starts from the edges and corners where the coordination numbers are lower than at other positions because the lower activation energy of these sites makes them more mobile, which is also in accordance with a computer simulation study.<sup>43</sup> Moreover, the coated Au NTs are much more stable than bare Au NTs due in part to a reduction of surface diffusion of the surface Au atoms caused by the coating layers<sup>39</sup> (mSiO<sub>2</sub> or carbon layers, which apparently also bring the diffusion to a halt) in combination with a reduction in the surface free-energy of the Au particles by the silica layers. Both the lowering of the activation energy for diffusion and the slowed down atomic surface diffusion in combination with a reduction in the thermodynamic driving force, are in agreement with the previous investigation of Au NRs.<sup>21</sup> It is likely that the stronger stabilizing effect of the increased shell thickness is due to the fact that it will cost more energy to deform thicker shells to accommodate the changing Au NP shape inside the shells. We already mentioned that we think that the fact that the mesoporous silica becomes non-porous

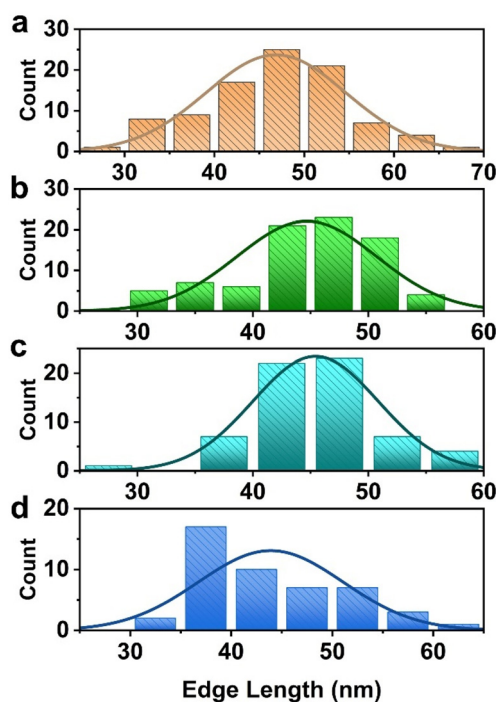


Fig. 5 Size distribution of Au NT@mSiO<sub>2</sub> CS and YS NPs after heating at 600 °C in an oven in air. (a) Au NT@mSiO<sub>2</sub> YS-30; (b) Au NT@mSiO<sub>2</sub> CS-20 nm; (c) Au NT@mSiO<sub>2</sub> YS-20 nm; (d) Au NT@mSiO<sub>2</sub> CS-10 nm.

combined with the flat shape of the NTs might explain the extra stability that the mesoporous silica layers provide to this particle shape as compared to for example Au NRs. However, the above reasoning does not explain the comparable stability of NTs with a yolk-shell structure as compared to the core-shell systems. Based also on the results explained in ref. 40 where extraordinary stability against deformations at high temperature even towards the bulk melting point of Au could be induced by just a thin  $\sim$ nm thick layer of carbon, we can only conclude that we think that a thicker and higher density SiO<sub>2</sub> shell in the YS-30 systems covered one plane face and partial of edges of Au NTs preventing the diffusion of the Au atoms up to high temperatures.

## Conclusions

In summary, we investigated the thermal stability of the Au NTs without and with different mSiO<sub>2</sub> confining and ligand shells. Due to the atoms' position-related energy barriers for diffusion, the Au NTs start to deform from the corners and edges where the atoms' coordination number is lower than at other positions, and the temperature for which deformations became noticeable on an hour time scale is at around 200 °C for the NPs in the present study when the particles were without an external confining shell. Upon increasing the heating temperature, the Au NTs were found to become more sphere-like particles *via* surface diffusion of Au atoms to reduce the surface energy of the overall particle. The LSPR band of Au NTs showed blue shifts when the particles deformed by shortening of the edge length and increasing of the thickness, finally shifting to around 570 nm which corresponds to the LSPR peak position for Au nanospheres. Surprisingly, we also found that Au NT@mSiO<sub>2</sub> YS NPs with a yolk-shell morphology which at first observation appeared with not all sides of the Au NP covered by a (porous) silica layer were as stable as Au NT@mSiO<sub>2</sub> CS NPs with a core-shell morphology where most of the Au surface was clearly covered. We hypothesize that the Au NTs inside these yolk-shell systems are also covered on the Au NP sides facing away from the more easily visible silica layer forming the outside of the YS morphology. Less surprising is that the thermal stability of Au NT@mSiO<sub>2</sub> CS NPs was enhanced when the thickness of a mSiO<sub>2</sub> shell that was completely covering the Au NTs was increased from  $\sim$ 10 to 20 nm. Our findings here may inspire the use of metal@mSiO<sub>2</sub> yolk-shell particles as a stable surface enhanced Raman (SERS) sensor for high-temperature reactions. Future work using these YS systems also for catalysis may show an enhancement in both activity and stability due to the nanoconfinement effect.

## Experimental section

Experimental details are given in the ESI.†

## Author contributions

X. X. designed and performed all the experiments and FDTD simulations and wrote the first draft of the manuscript. W. A. helped to design and perform the initial *in situ* heating experiments. M. A. v. H. and A. v. B. designed and supervised the project. All authors participated in writing and revising the manuscript.

## Conflicts of interest

The authors declare there is no conflict of interest.

## Acknowledgements

We thank Dr Da Wang and Dr Jessi van der Hoeven for the fruitful discussions. Dr Ting Yu from the CMI group is acknowledged for helping with the oven settings. X. X., M. A. v. H. and A. v. B. acknowledge the financial support from EU H2020-MSCA-ITN-2015 project 'MULTIMAT' (project number: 676045).

## References

- 1 L. Scarabelli, M. Coronado-Puchau, J. J. Giner-Casares, J. Langer and L. M. Liz-Marzán, Monodisperse Gold Nanotriangles Size Control, Large-Scale Self-Assembly, and Performance in Surface-Enhanced Raman Scattering, *ACS Nano*, 2014, **8**, 5833–5842.
- 2 G. Wang, Y. Liu, C. Gao, L. Guo, M. Chi, K. Ijio, M. Maeda and Y. Yin, Island Growth in the Seed-Mediated Overgrowth of Monometallic Colloidal Nanostructures, *Chem*, 2017, **3**(4), 678–690.
- 3 S. R. Bhattarai, P. J. Derry, K. Aziz, P. K. Singh, A. M. Khoo, A. S. Chadha, A. Liopo, E. R. Zubarev and S. Krishnan, Gold nanotriangles: scale up and X-ray radiosensitization effects in mice, *Nanoscale*, 2017, **9**(16), 5085–5093.
- 4 M. Chen, S. Tang, Z. Guo, X. Wang, S. Mo, X. Huang, G. Liu and N. Zheng, Core-shell Pd@Au nanoplates as theranostic agents for *in vivo* photoacoustic imaging, CT imaging, and photothermal therapy, *Adv. Mater.*, 2014, **26**(48), 8210–8216.
- 5 Z. Lou, M. Fujitsuka and T. Majima, Pt-Au Triangular Nanoprisms with Strong Dipole Plasmon Resonance for Hydrogen Generation Studied by Single-Particle Spectroscopy, *ACS Nano*, 2016, **10**(6), 6299–6305.
- 6 N. M. Andoy, X. Zhou, E. Choudhary, H. Shen, G. Liu and P. Chen, Single-molecule catalysis mapping quantifies site-specific activity and uncovers radial activity gradient on single 2D nanocrystals, *J. Am. Chem. Soc.*, 2013, **135**(5), 1845–1852.
- 7 Z. Fan, Y. Zhu, X. Huang, Y. Han, Q. Wang, Q. Liu, Y. Huang, C. L. Gan and H. Zhang, Synthesis of ultrathin face-centered-cubic Au@Pt and Au@Pd core-shell nano-

- plates from hexagonal-close-packed to square sheets, *Angew. Chem., Int. Ed.*, 2015, **54**(19), 5672–5676.
- 8 C. Kan, G. Wang, X. Zhu, C. Li and B. Cao, Structure and thermal stability of gold nanoplates, *Appl. Phys. Lett.*, 2006, **88**(7), 071904.
  - 9 W. Albrecht, S. Van Aert and S. Bals, Three-Dimensional Nanoparticle Transformations Captured by an Electron Microscope, *Acc. Chem. Res.*, 2021, **54**(5), 1189–1199.
  - 10 X. Zhang, S. Han, B. Zhu, G. Zhang, X. Li, Y. Gao, Z. Wu, B. Yang, Y. Liu, W. Baaziz, O. Ersen, M. Gu, J. T. Miller and W. Liu, Reversible loss of core-shell structure for Ni–Au bimetallic nanoparticles during CO<sub>2</sub> hydrogenation, *Nat. Catal.*, 2020, **3**(4), 411–417.
  - 11 Z. Fan, L. Zhang, D. Baumann, L. Mei, Y. Yao, X. Duan, Y. Shi, J. Huang, Y. Huang and X. Duan, In Situ Transmission Electron Microscopy for Energy Materials and Devices, *Adv. Mater.*, 2019, **31**(33), e1900608.
  - 12 B. Zhu, J. Meng, W. Yuan, X. Zhang, H. Yang, Y. Wang and Y. Gao, Reshaping of Metal Nanoparticles Under Reaction Conditions, *Angew. Chem., Int. Ed.*, 2020, **59**(6), 2171–2180.
  - 13 T. Xu and L. Sun, Dynamic *In situ* Experimentation on Nanomaterials at the Atomic Scale, *Small*, 2015, **11**(27), 3247–3262.
  - 14 J. E. S. van der Hoeven, J. Jelic, L. A. Olthof, G. Totarella, R. J. A. van Dijk-Moes, J. M. Krafft, C. Louis, F. Studt, A. van Blaaderen and P. E. de Jongh, Unlocking synergy in bimetallic catalysts by core-shell design, *Nat. Mater.*, 2021, **20**(9), 1216–1220.
  - 15 A. Pedraza-Tardajos, E. Arslan Irmak, V. Kumar, A. Sanchez-Iglesias, Q. Chen, M. Wirix, B. Freitag, W. Albrecht, S. Van Aert, L. M. Liz-Marzan and S. Bals, Thermal Activation of Gold Atom Diffusion in Au@Pt Nanorods, *ACS Nano*, 2022, **16**(6), 9608–9619.
  - 16 W. Albrecht, E. Bladt, H. Vanrompay, J. D. Smith, S. E. Skrabalak and S. Bals, Thermal Stability of Gold/Palladium Octopods Studied *In Situ* in 3D: Understanding Design Rules for Thermally Stable Metal Nanoparticles, *ACS Nano*, 2019, **13**(6), 6522–6530.
  - 17 A. Skorikov, W. Albrecht, E. Bladt, X. Xie, J. E. S. van der Hoeven, A. van Blaaderen, S. Van Aert and S. Bals, Quantitative 3D Characterization of Elemental Diffusion Dynamics in Individual Ag@Au Nanoparticles with Different Shapes, *ACS Nano*, 2019, **13**(11), 13421–13429.
  - 18 S. Dai, Y. Hou, M. Onoue, S. Zhang, W. Gao, X. Yan, G. W. Graham, R. Wu and X. Pan, Revealing Surface Elemental Composition and Dynamic Processes Involved in Facet-Dependent Oxidation of Pt(3)Co Nanoparticles via *In Situ* Transmission Electron Microscopy, *Nano Lett.*, 2017, **17**(8), 4683–4688.
  - 19 K. Koga, T. Ikeshoji and K. Sugawara, Size- and temperature-dependent structural transitions in gold nanoparticles, *Phys. Rev. Lett.*, 2004, **92**(11), 115507.
  - 20 A. S. Barnard, X. M. Lin and L. A. Curtiss, Equilibrium morphology of face-centered cubic gold nanoparticles >3 nm and the shape changes induced by temperature, *J. Phys. Chem. B*, 2005, **109**(51), 24465–24472.
  - 21 W. J. Kennedy, S. Izor, B. D. Anderson, G. Frank, V. Varshney and G. J. Ehlert, Thermal Reshaping Dynamics of Gold Nanorods: influence of size, shape, and local environment, *ACS Appl. Mater. Interfaces*, 2018, **10**, 43865–43873.
  - 22 A. B. Taylor, A. M. Siddiquee and J. W. Chon, Below melting point photothermal reshaping of single gold nanorods driven by surface diffusion, *ACS Nano*, 2014, **8**(12), 12071–12079.
  - 23 Y. Bai, C. Gao and Y. Yin, Fully alloyed Ag/Au nanorods with tunable surface plasmon resonance and high chemical stability, *Nanoscale*, 2017, **9**(39), 14875–14880.
  - 24 W. Albrecht, J. E. van der Hoeven, T. S. Deng, P. E. de Jongh and A. van Blaaderen, Fully alloyed metal nanorods with highly tunable properties, *Nanoscale*, 2017, **9**(8), 2845–2851.
  - 25 S. H. Joo, J. Y. Park, C. K. Tsung, Y. Yamada, P. Yang and G. A. Somorjai, Thermally stable Pt/mesoporous silica core-shell nanocatalysts for high-temperature reactions, *Nat. Mater.*, 2009, **8**(2), 126–131.
  - 26 P. Buffat and J. P. Borel, Size effect on the melting temperature of gold particles, *Phys. Rev. A*, 1976, **13**(6), 2287–2298.
  - 27 K. Dick, T. Dhanasekaran, Z. Zhang and D. Meisel, Size-Dependent Melting of Silica-Encapsulated Gold Nanoparticles, *J. Am. Chem. Soc.*, 2002, **124**(10), 2312.
  - 28 R. Wang and D. Kuroski, Thermal Reshaping of Gold Microplates: Three Possible Routes and Their Transformation Mechanisms, *ACS Appl. Mater. Interfaces*, 2019, **11**(44), 41813–41820.
  - 29 H. Cho, J. W. Shin and R. Ryoo, Atomic Scale Mechanisms Underlying Thermal Reshaping of Anisotropic Gold Nanocrystals Revealed by *In Situ* Electron Microscopy, *J. Phys. Chem. C*, 2020, **124**(23), 12855–12863.
  - 30 C. Zhu, S. Zhao, Z. Fan, H. Wu, F. Liu, Z. Chen and A. Li, Confinement of CoP Nanoparticles in Nitrogen-Doped Yolk-Shell Porous Carbon Polyhedron for Ultrafast Catalytic Oxidation, *Adv. Funct. Mater.*, 2020, **30**(49), 20033947.
  - 31 C. Wang, Y. Qiu, X. Zhang, Y. Zhang, N. Sun and Y. Zhao, Geometric design of a Ni@silica nano-capsule catalyst with superb methane dry reforming stability: enhanced confinement effect over the nickel site anchoring inside a capsule shell with an appropriate inner cavity, *Catal. Sci. Technol.*, 2018, **8**(19), 4877–4890.
  - 32 C. Yu and J. He, Synergic catalytic effects in confined spaces, *Chem. Commun.*, 2012, **48**(41), 4933–4940.
  - 33 G. Prieto, H. Tuysuz, N. Duyckaerts, J. Knossalla, G. H. Wang and F. Schuth, Hollow Nano- and Microstructures as Catalysts, *Chem. Rev.*, 2016, **116**(22), 14056–14119.
  - 34 Y. Zhong, X. Kong, Z. Song, Y. Liu, L. Peng, L. Zhang, X. Luo, J. Zeng and Z. Geng, Adjusting Local CO Confinement in Porous-Shell Ag@Cu Catalysts for Enhancing C-C Coupling toward CO(2) Electroreduction, *Nano Lett.*, 2022, **22**(6), 2554–2560.

- 35 A. B. Grommet, M. Feller and R. Klajn, Chemical reactivity under nanoconfinement, *Nat. Nanotechnol.*, 2020, **15**(4), 256–271.
- 36 D. Wang, C. Zhang, L. Zhang, X. Xie and Y. Lv, Integrated Optimization of Crystal Facets and Nanoscale Spatial Confinement toward the Boosted Catalytic Performance of Pd Nanocrystals, *Inorg. Chem.*, 2024, **63**(2), 1247–1257.
- 37 X. Xie, M. A. van Huis and A. van Blaaderen, Single-step coating of mesoporous SiO<sub>2</sub> onto nanoparticles: growth of yolk-shell structures from core-shell structures, *Nanoscale*, 2021, **13**(24), 10925–10932.
- 38 H. Chen, M. Tian, L. Zhao, F. Wang, L. Sun, J. Wang and C. Yan, Plasmon–molecule interactions, *Nano Today*, 2010, (5), 494–505.
- 39 W. Albrecht, A. van de Glind, H. Yoshida, Y. Isozaki, A. Imhof, A. van Blaaderen, P. E. de Jongh, K. P. de Jong, J. Zecevic and S. Takeda, Impact of the electron beam on the thermal stability of gold nanorods studied by environmental transmission electron microscopy, *Ultramicroscopy*, 2018, **193**, 97–103.
- 40 W. Albrecht, T. S. Deng, B. Goris, M. A. van Huis, S. Bals and A. van Blaaderen, Single Particle Deformation and Analysis of Silica-Coated Gold Nanorods before and after Femtosecond Laser Pulse Excitation, *Nano Lett.*, 2016, **16**(3), 1818–1825.
- 41 M. N. O'Brien, M. R. Jones, K. L. Kohlstedt, G. C. Schatz and C. A. Mirkin, Uniform circular disks with synthetically tailorable diameters: two-dimensional nanoparticles for plasmonics, *Nano Lett.*, 2015, **15**(2), 1012–1017.
- 42 B. Molleman and T. Hiemastra, Size and shape dependency of the surface energy of metallic nanoparticles unifying the atomic and thermodynamic approaches, *Phys. Chem. Chem. Phys.*, 2018, **20**, 20575–20587.
- 43 X. He, F. Cheng and Z. X. Chen, The Lattice Kinetic Monte Carlo Simulation of Atomic Diffusion and Structural Transition for Gold, *Sci. Rep.*, 2016, **6**, 33128.